Chemistry–A European Journal
Research Article
doi.org/10.1002/chem.202104319
Chemistry Europe
European Chemical Societies Publishing
www.chemeurj.org

Add a Pinch of Tetrel: The Transformation of a Centrosymmetric Metal into a Nonsymmorphic and Chiral Semiconductor

Shannon J. Lee,[a, b] Gayatri Viswanathan,[a, b] Scott L. Carnahan,[a, b] Colin P. Harmer,[a, b] Georgiy Akopov,[a, b] Aaron J. Rossini,[a, b] Gordon J. Miller,[a] and Kirill Kovnir*[a, b]

Abstract: Centrosymmetric skutterudite RhP_3 was converted to a nonsymmorphic and chiral compound $RhSi_{0.3}P_{2.7}$ (space group $P2_12_12_1$) by means of partial replacement of Si for P. The structure, determined by a combination of X-ray crystallography and solid state ^{31}P NMR, exhibits branched polyanionic P/Si chains that are unique among metal phosphides. A driving force to stabilize the locally non-centrosymmetric *cis*-$RhSi_2P_4$ and *fac*-$RhSi_3P_3$ fragments is π-electron back-donation between the Rh t_{2g}-type orbitals and the unoccupied antibonding Si/P orbitals, which is more effective for Si than for P. In situ studies and total energy calculations revealed the metastable nature of $RhSi_{0.3}P_{2.7}$. Electronic structure calculations predicted centrosymmetric cubic RhP_3 to be metallic which was confirmed by transport properties measurements. In contrast, the electronic structure for chiral orthorhombic $RhSi_{0.3}P_{2.7}$ contained a bandgap, and this compound was shown to be a narrow gap semiconductor.

Introduction

The discovery of noncentrosymmetric (NCS) and nonsymmorphic materials is crucial for the advancement of emergent technologies. Symmetry-driven physical phenomena, such as second harmonic generation and topological non-trivial properties are only a sliver of the applications for new NCS materials.[1–9] Ternary silicon phosphides, such as $Ba_2Si_3P_6$, $MnSiP_2$, and $RuSi_4P_4$ have shown promising nonlinear optical properties,[10–14] and have prompted the investigation of other metal tetrel pnictides.[15] Generally, NCS structures are rare in intermetallics (< 10%) but are much more prevalent (up to 95%) among transition metal silicon phosphides where $M/(Si+P) < 1$.[16] Compared to binary metal pnictides, metal tetrel pnictides (*M*–*Tt*–*Pn*) have additional structural flexibility due to *M*–*Tt* covalent bonding, which leads to the predominance of NCS structures.[14,17] When the metal has a similar electronegativity as the main group elements, both *M*–*Tt* and *M*–*Pn* bonding can occur.[18–22] In contrast, in Zintl phase tetrel pnictides such as $Ba_2Si_3P_6$, a strongly electropositive metal *A* (usually alkali or alkaline-earth cation) is coordinated only by the more electronegative *Pn* atoms; therefore, the tetrel is always coordinated by *Pn* and no *A*–*Tt* polar covalent bonds are present.[11,23–25]

The arrangement of tetrel and pnictogen atoms around 4*d* and 5*d* transition metals results in local NCS coordination in several ternary *M*–*Tt*–*Pn* phases. Common NCS fragments include *fac*-[*M*@Si_3P_3] octahedral units found in $RuSi_4P_4$ and $IrSi_3P_3$, as well as linear [Si–Au–P] and square planar *cis*-[Au@Ge_2P_2] fragments found in gold tetrel pnictides.[17,19] We hypothesize that the presence of two types of covalent bonds, i.e., *M*–Si and *M*–P, favors the formation of NCS structures. To verify this hypothesis, we performed Si substitutions for P atoms in the centrosymmetric skutterudite, RhP_3.

Centrosymmetric skutterudites MPn_3, crystallizing in the cubic space group $Im\bar{3}$, have been extensively studied for their use as thermoelectric materials.[26–33] A partial or full replacement of pnictogen atoms with Ge in the skutterudite structures has been reported.[34–37] Many skutterudites can be electronically tuned by means of aliovalent substitution. Additionally, structures with heavier 4*d* and 5*d* transition metals showing strong spin-orbit coupling are predicted to have band crossings and topologically non-trivial properties useful for quantum computing.[38,39] Filled skutterudites further expand this family of compounds with potential thermoelectric applications and introduce unique electronic and magnetic properties including metal-insulator transitions and superconductivity.[36,37,40,41]

Skutterudites containing heavier metals, such as Rh, have been predicted to be metallic or semi-metallic, depending on the computational method used.[42,43] The study herein describes the

[a] Dr. S. J. Lee, G. Viswanathan, Dr. S. L. Carnahan, Dr. C. P. Harmer, Dr. G. Akopov, Prof. Dr. A. J. Rossini, Prof. Dr. G. J. Miller, Prof. Dr. K. Kovnir
Department of Chemistry
Iowa State University
50011 Ames, IA (USA)
E-mail: kovnir@iastate.edu

[b] Dr. S. J. Lee, G. Viswanathan, Dr. S. L. Carnahan, Dr. C. P. Harmer, Dr. G. Akopov, Prof. Dr. A. J. Rossini, Prof. Dr. K. Kovnir
Ames Laboratory, US DOE
50011 Ames, IA (USA)

Supporting information for this article is available on the WWW under https://doi.org/10.1002/chem.202104319

major structural transformations and property modifications upon substituting 10% of P atoms with Si in RhP_3. The novel metastable compound $RhSi_{0.3}P_{2.7}$ crystallizes in the NCS, chiral, nonsymmorphic, orthorhombic space group $P2_12_12_1$ and undergoes a high-temperature phase transformation into the stable centrosymmetric cubic $Im\bar{3}$ structure of the same composition. The synthesis of $RhSi_{0.3}P_{2.7}$, structure determination via single crystal X-ray diffraction (SCXRD) and magic angle spinning (MAS) ^{31}P solid-state NMR spectroscopy, transport properties, and computational investigation for Si site preferences are reported.

Results and Discussion

Synthesis

Upon analyzing a sample with nominal composition $RhSi_3P_3$ via powder X-ray diffraction (PXRD), numerous unidentified peaks indicated formation of a new phase, which was subsequently established to be the novel NCS orthorhombic phase $RhSi_{0.3}P_{2.7}$ by means of single crystal X-ray diffraction (SCXRD). The ability to distinguish Si from P via SCXRD is limited due to their similar X-ray scattering factors (see Supporting Information). Solid state ^{31}P NMR and energy dispersive X-ray (EDS) spectroscopies were employed to confirm structure and composition, respectively. The synthesis of this new phase is most successful when the source of Rh metal (either commercial Rh powder or $RhCl_3$) is reduced under a flow of H_2 to form fine Rh metal particles with oxide-free surfaces. Stoichiometric ratios of elements were reacted in the range of 1073–1173 K to produce dark gray powders of $RhSi_{0.3}P_{2.7}$ with minute amounts of RhP_3 admixture. Detailed experimental methods are provided in the Supporting Information. For clarity, the following nomenclature will be used to identify the phases discussed: *o*-$RhSi_{0.3}P_{2.7}$ = orthorhombic $RhSi_{0.3}P_{2.7}$ crystallizing in $P2_12_12_1$ space group; *o*-RhP_3 = hypothetical orthorhombic RhP_3 crystallizing in $P2_12_12_1$ space group; *c*-$RhSi_{0.3}P_{2.7}$ = skutterudite-type cubic $RhSi_{0.3}P_{2.7}$ crystallizing in $Im\bar{3}$; and *c*-RhP_3 = skutterudite-type cubic RhP_3.

Crystal structures

c-RhP_3 crystallizes in the skutterudite structure type, space group $Im\bar{3}$ (No. 204). The crystal structure may be described as vertex-sharing RhP_6 octahedral units that are tilted to create P–P bonds forming P_4 squares (Figure 1). This recognizable structure type has been extensively studied. When a small amount of Si is introduced in place of P in *c*-RhP_3, a NCS orthorhombic compound (*o*-$RhSi_{0.3}P_{2.7}$) forms and crystallizes in the chiral nonsymmorphic space group $P2_12_12_1$ (No. 19) with $Z = 8$, Pearson symbol *oP*32, and Wyckoff sequence a^8. Deposition Number 2086605 (for $RhSi_{0.3}P_{2.7}$) contain(s) the supplementary crystallographic data for this paper. These data are provided free of charge by the joint Cambridge Crystallographic Data Centre and Fachinformationszentrum Karlsruhe Access Structures service.

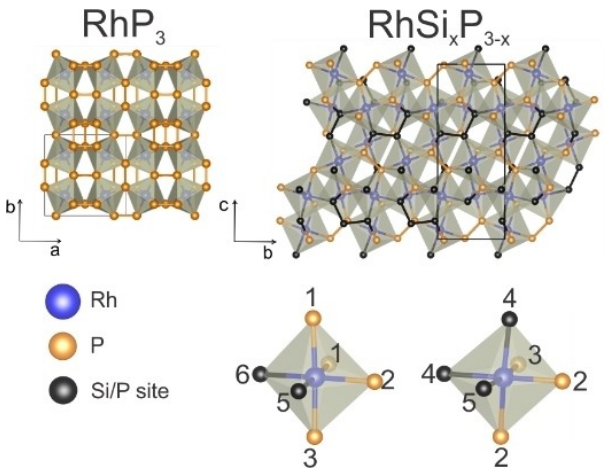

Figure 1. Crystal structures of (left) *c*-RhP_3 ($Im\bar{3}$) and (right) *o*-$RhSi_{0.3}P_{2.7}$ ($P2_12_12_1$) showing the octahedral coordination of the Rh atoms (blue) surrounded by P (orange) and mixed Si/P sites (black), with unit cells outlined in thin black lines.

The crystal structure of *o*-$RhSi_{0.3}P_{2.7}$ has 2 Rh sites, 3 fully occupied P sites, and 3 mixed Si/P sites. The structure can be described as Rh atoms octahedrally coordinated by Si and P atoms, which are connected by Si–P or P–P branches. There are two types of distorted octahedral units throughout the structure (Figure 1): one Rh is coordinated by 2 mixed Si/P sites (black atoms) in *cis*-positions and 4 fully occupied P atoms (orange atoms), while the other Rh is coordinated by 3 mixed sites and 3 fully occupied P atom sites in a *facial* coordination geometry. Packing of these NCS octahedral units gives rise to its overall NCS crystal structure. The preference for *cis*- and *fac*- arrangements of Si and P coordination sites around Rh may be due to differences between Rh–Si and Rh–P π-type interactions within the octahedral units. As ligands in the octahedral units, Si and P are both π-donor ligands to Rh arising from the occupied Si–P and P–P orbitals. π-electron back donation between the t_{2g}-type orbitals of Rh and the unoccupied (antibonding) orbitals of the Si/P is more effective for Rh–Si than Rh–P contacts. These subtle orbital interactions result in a preferred *cis*- rather than *trans*- geometry. The same concept may also contribute to the observation of shorter *M*-Si bonds as compared to the *M*–P bonds in other reported metal silicon phosphides.[14]

The P/Si polyanion in the crystal structure of *o*-$RhSi_{0.3}P_{2.7}$ is a branched 1D chain running along the [100] direction (Figure 2). Each chain is composed of atoms of differing connectivity in the polyanion. The three unique types of P atoms in the structure can be described as *terminal* 1b-P atoms only connected to a single other Si/P (P2 site), *linker* 2b-P atoms connected to two other Si/P sites (P1, P3, P4, and P5 sites), and *branching* 3b-P atoms connected by three other Si/P sites (P6 site) (Tables S1 and S2). Rh–Si and Rh–P bonds complete the distorted tetrahedral coordination of each nonmetal atom. In the 1D chains, 3 sites are occupied solely by P (orange atoms), and 3 sites are mixed Si/P sites (black sites).

Further investigation was needed to confirm the assignment of the formally anionic sites in this structure due to the similar

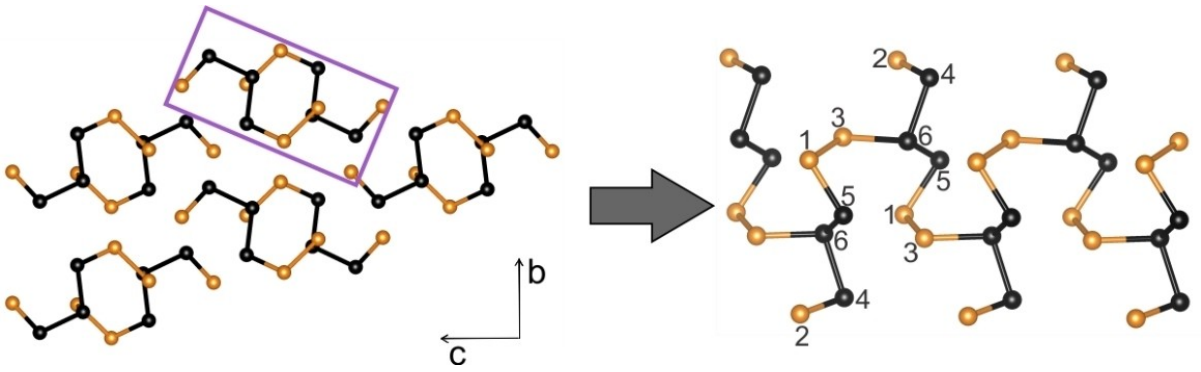

Figure 2. Two different viewpoints of (Si/P) 1D chains in the *o*-$RhSi_{0.3}P_{2.7}$ structure. Left: Packing of the chains which run along the [100] direction. Right: Side view of a single polyanion chain with crystallographic sites labeled. Fully occupied P sites are shown in orange while mixed Si/P sites are shown in black.

X-ray scattering factors of Si and P. ^{31}P fast magic angle spinning solid-state nuclear magnetic resonance (MAS SS NMR) experiments were performed on *c*-RhP_3 (Figure 3A) and *o*-$RhSi_{0.3}P_{2.7}$ (Figure 3B–G) samples to probe the P sites in the latter structure. At a slow MAS frequency of 8 kHz, the ^{31}P NMR spectrum of *o*-$RhSi_{0.3}P_{2.7}$ is obscured by overlapping spinning sidebands due to the ^{31}P chemical shift anisotropy (CSA) of the different sites (Figure S1). However, using a smaller diameter rotor and increasing the spinning rate to 25 or 50 kHz MAS removes most spinning sidebands and unambiguously shows that there are at least four unique ^{31}P sites in the studied sample (Figure 3B–G). The ^{31}P NMR spectra show significant inhomogeneous broadening of the peaks, likely because of the combined effects of susceptibility broadening and structural disorder due to mixed occupancy of P/Si sites. Inhomogeneous broadening can be partly removed by taking slices out of a 2D spectrum, in this case a ^{31}P–^{31}P exchange spectroscopy (EXSY) spectrum (Figure 3C–G).[44–46]

The ^{31}P isotropic chemical shifts of *o*-$RhSi_{0.3}P_{2.7}$ are observed between ca. 100 ppm and 450 ppm, consistent with the chemical shifts reported for a variety of other semiconducting and metallic transition metal phosphides.[47–49] The peak visible at 363 ppm in the spectrum of *o*-$RhSi_{0.3}P_{2.7}$ is from a RhP_3 impurity, which leaves three ^{31}P NMR signals at 306 ppm, 199 ppm and 111 ppm attributed to *o*-$RhSi_{0.3}P_{2.7}$. The differences in ^{31}P chemical shifts likely arise due to the different types

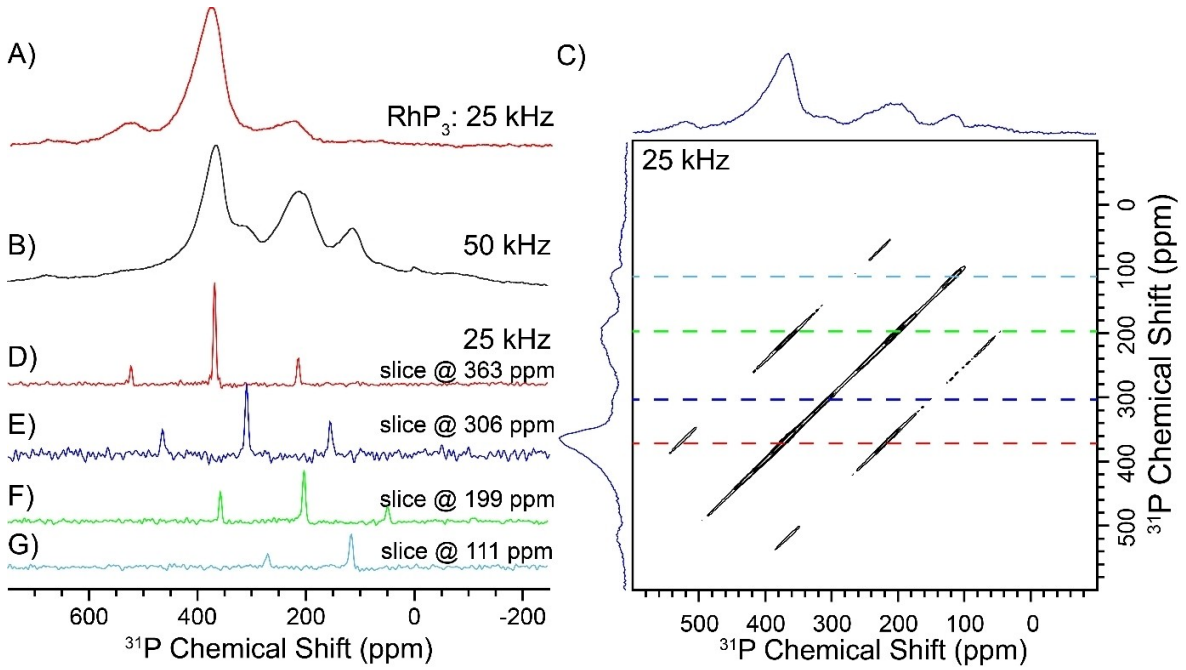

Figure 3. (A) MAS ^{31}P solid-state NMR spectrum of RhP_3 obtained with a 25 kHz MAS frequency. (B) MAS ^{31}P solid-state NMR spectrum of *o*-$RhSi_{0.3}P_{2.7}$ sample obtained with 50 kHz MAS frequency. (C) 2D ^{31}P–^{31}P exchange spectroscopy (EXSY) spectrum of *o*-$RhSi_{0.3}P_{2.7}$ sample obtained with a MAS frequency of 25 kHz. (D–G) shows the rows extracted at indirect dimension chemical shifts of 363, 306, 199, and 111 ppm. Spinning sidebands are visible to the sides of each of the isotropic signals.

of connectivity of the P atoms to its neighbors, similar to other NMR structural analyses.[14,24,50] The relative signal integration ratio is 65:21:15 for the peaks at 199 ppm, 111 ppm, and 306 ppm, respectively. The most intense peak slice at 199 ppm should correspond to the *linker* 2*b*-P atoms (P1, P3, P5, and P4, Figure 2) which make up ca. two thirds of the possible P sites, in agreement with the integrated intensity. The remaining one third of the possible P sites are split between the *terminal* P2 site, which has 100% P occupancy, and the *branching* P6 site, which has only 76% of P. Based on peak intensities we assign the resonance at 306 ppm to P6 and the one at 111 ppm to P2.

To the best of our knowledge, the 1D polyanionic chain found in *o*-$RhSi_{0.3}P_{2.7}$ is unique, even if considered to be composed of solely P atoms.[51–53] Although ThP_7 crystallizes in the same space group and Wyckoff sequence ($P2_12_12_1$ and a^8), the P polyanion is different. In the crystal structure of ThP_7 the polyanion is a 3D framework with two-bonded (2*b*)- and three-bonded (3*b*)-P atoms,[54] while the 1D polyanion of *o*-$RhSi_{0.3}P_{2.7}$ is composed of 1*b*-, 2*b*-, and 3*b*-P/Si atoms. Thorium also exhibits a larger coordination number of 8–10,[54] while Rh is octahedrally coordinated by 6 Si/P atoms in the crystal structure of *o*-$RhSi_{0.3}P_{2.7}$. Furthermore, in the phosphides ReP_3 and RuP_3 with octahedral coordination of Re and Ru, branched 1D polyanions with 1*b*-, 2*b*-, and 3*b*-P atoms are present with formal charges of −3 per P_3 unit.[55,56] However, both such polyanions are different from the one found in *o*-$RhSi_{0.3}P_{2.7}$ (Figure S2).

The bond distances found in the polyanion of *o*-$RhSi_{0.3}P_{2.7}$ structure are shown in Figure S3 and range from 2.18–2.30 Å, with the longest bond being between the fully occupied P sites (P1–P3). These bond distances fall within the P–P bond range of other metal phosphides with chains, as in RuP_3 (2.18–2.23 Å)[55] and ReP_3 (2.20–2.22 Å),[56] and within the Si–P bond range of ternary phases such as $RuSi_4P_4$ (2.21–2.32 Å)[14] and Ag_2SiP_2 (2.25 Å).[19]

Considering the formal charge of the polyanion, if all atoms are assumed to be P, 3*b*-P have formal 0 oxidation state while 2*b*- and 1*b*-P atoms have formal oxidation states −1 and −2, respectively. The overall polyanion charge then is $(Rh^{3+})_2(1b\text{-}P)^{2-}(2b\text{-}P)^{1-}{}_4(3b\text{-}P)^0$. Every replacement of P with Si should result in an overall increase of the charge by 1 per Si. However, we have shown that this ionic electron-counting approach, which works well for Zintl-like phosphides of d^{10} metals,[50,53,57–59] is not applicable for 4*d* and 5*d* transition metal phosphides and silicides with strong covalent *M*–P and *M*-Si bonding.[14,17]

Polymorphic phase transformation

Heat treatment of the pre-synthesized *o*-$RhSi_{0.3}P_{2.7}$ sample at high temperatures revealed a structural transformation from the orthorhombic $P2_12_12_1$ structure to the skutterudite type $Im\bar{3}$ structure. No significant thermal effects are observed in the DSC experiment up to 1373 K (Figure S4), probably due to insufficient sensitivity of the DSC method. The in situ synchrotron PXRD study, in addition to in-house ex situ experiments, further supported the irreversible nature of the *o*-$RhSi_{0.3}P_{2.7}$ to *c*-$RhSi_{0.3}P_{2.7}$ transformation (Figure 4).

The temperature dependent in situ PXRD experiment was performed on a sample containing *o*-$RhSi_{0.3}P_{2.7}$ and a small *c*-RhP_3 admixture (Figure 4A). The *o*-$RhSi_{0.3}P_{2.7}$ phase began to transform into *c*-$RhSi_{0.3}P_{2.7}$ at ~1300 K and upon cooling, we observed the orthorhombic phase peaks decreased in intensity while the skutterudite peaks increased until, finally, the skutterudite was the main phase (Figures 4B and S5). The structural transformation was irreversible as evident in Figure 4B. Absolute temperatures from the in situ setup can be inaccurate and obscured by kinetics of the transformation, therefore ex situ experiments were also conducted. The beginning of the orthorhombic→skutterudite transformations were observed as low as 873 K, with increasing skutterudite:orthorhombic ratio with annealing temperature. The ex situ experiments show that *o*-$RhSi_{0.3}P_{2.7}$ fully converts to the *c*-

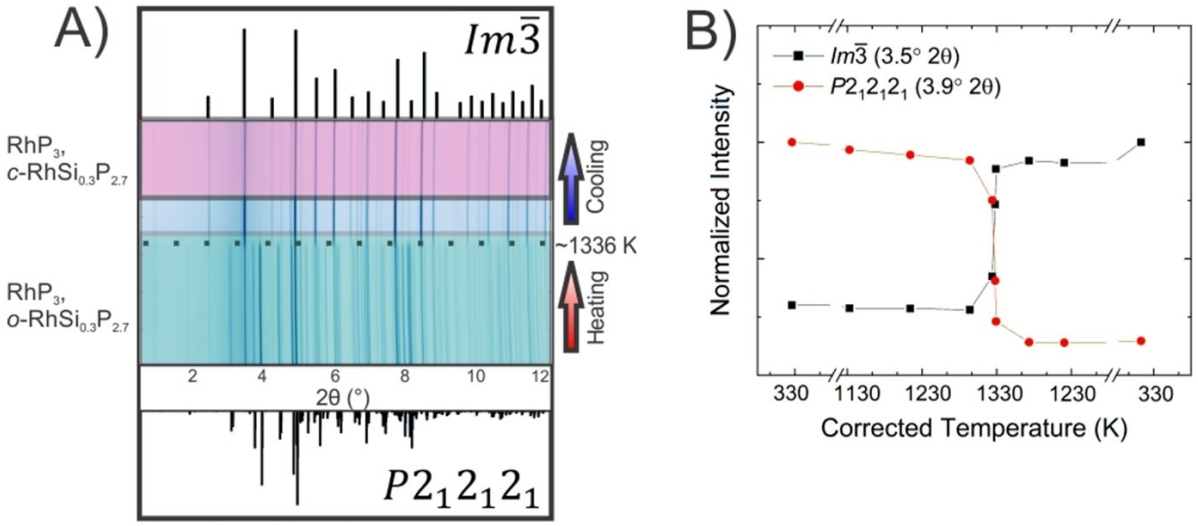

Figure 4. Transformation from *o*-$RhSi_{0.3}P_{2.7}$ to *c*-$RhSi_{0.3}P_{2.7}$ at ~1300 K from 17-BM in situ PXRD ($\lambda = 0.24153$ Å). **A**: Contour plot highlighting phase transformation and **B**: intensities of select PXRD peaks corresponding to *o*-$RhSi_{0.3}P_{2.7}$ (at 3.9° 2θ) and *c*-$RhSi_{0.3}P_{2.7}$ (at 3.5° 2θ) phases.

Rh$Si_{0.3}P_{2.7}$ upon annealing at 1273 K (Figure S6). Elemental analysis by EDS confirmed that, after the ex situ phase transformations, Si is retained in the skutterudite type structure. While EDS is a semi-quantitative method and exact quantification of Si/P ratio in a compound with a heavy metal is challenging without a proper standard,[14] the observed Si content in the orthorhombic phase, 0.14(2) per one Rh, was similar to the Si content in the high-temperature skutterudite phase, 0.13(3) per one Rh.

Although metastable *o*-$RhSi_{0.3}P_{2.7}$ can be synthesized by quenching from 1073 K, *c*-$RhSi_{0.3}P_{2.7}$ appears to be the more thermodynamically stable phase. To probe the energy landscape of these phases and Si-free RhP_3, computational coloring and total energy calculations were employed.

Atomic coloring and total energy calculations

To understand the thermodynamics of the orthorhombic→skutterudite phase transformation and the relative energies of both *o*-$RhSi_{0.3}P_{2.7}$ and *c*-$RhSi_{0.3}P_{2.7}$, a series of computational coloring and total energy calculations were conducted.[60] To evaluate site preferences for Si substitution in these structures, ordered crystal structures with Si substitution were developed and relative total energies of these models were compared. Ordered "Rh_8SiP_{23}" crystal structures were constructed for both the skutterudite and orthorhombic structure types by substituting one of 24 P sites with Si (4.2% Si). In the skutterudite-type structure, all main group element sites are equivalent, and the various models show a negligible difference in △E (Figure S7). However, in the orthorhombic structure, there is a strong preference for Si substitution in the 3-coordinate *branching* site, as seen by the lower energy models 21–24 (purple box in Figure 5, left), compared to the 2-coordinate *linker* (green boxes) and the 1-coordinate *terminal* sites (yellow box).

Since SCXRD data suggested a composition with 10% Si substitution, additional Si incorporation was considered by evaluating "$Rh_8Si_2P_{22}$" models (8.3% Si), which included the plausibility of homoatomic Si–Si bonds. Preferred Si atom positions for these models were in the *branching* and *linker* sites, and the relative energies of the crystal structures with Si–Si bonds were higher than those with only heteroatomic Si–P bonds. The calculated bond preferences agree with trends reported for other transition metal silicon phosphides, where homoatomic bonds are not observed even when the Si + P content is high (e.g., $RuSi_4P_4$).[14]

Finally, six ordered crystal structures "$Rh_8Si_3P_{21}$" (12.5% Si) were evaluated (Figure 5, right). Each of these model structures had Si atoms occupying one *branching* site and two *linker* sites. The SCXRD-determined crystal structure of *o*-$RhSi_{0.3}P_{2.7}$ is most similar to Model X, but the lowest energy "$Rh_8Si_3P_{21}$" crystal structure studied was Model Z. Nevertheless, the energy difference between Models X and Z is <2 meV/atom. In fact, all Models U–Z fall within 12 meV/atom of one another, indicating they are essentially equivalent at ambient temperatures because $k_BT = 25$ meV at room temperature (Table S3). This further supports the site preference for Si substitution in the higher coordinated sites within the polyanionic network of the orthorhombic structure, an outcome which agrees with chemical intuition.

Density of states

The density of states (DOS) for the two structure types (skutterudite and orthorhombic) were calculated to predict the electronic properties of "Rh_8P_{24}" (RhP_3) and "Rh_8SiP_{23}." The RhP_3

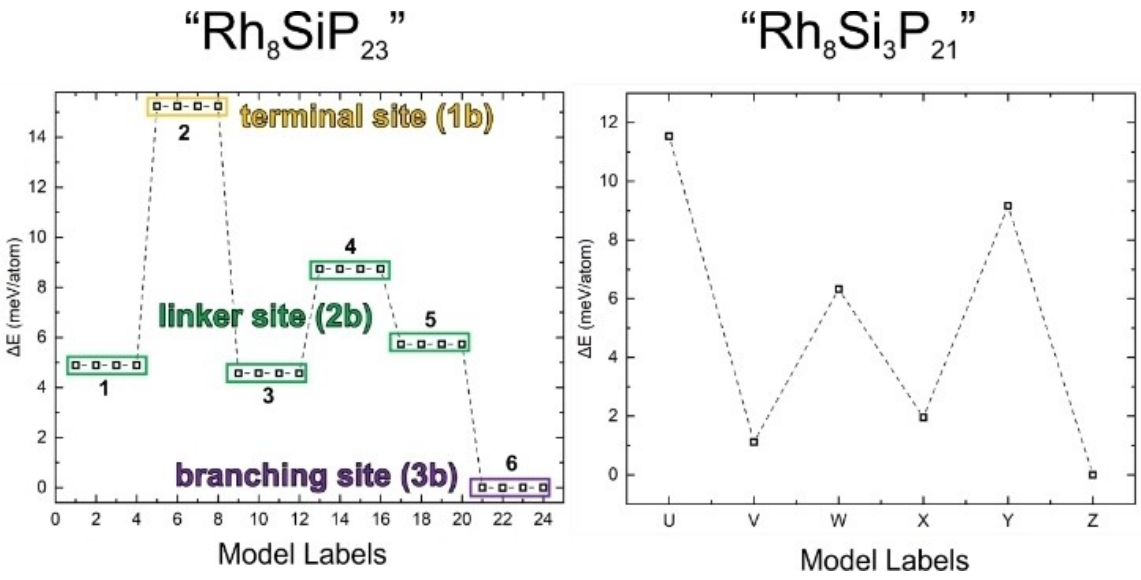

Figure 5. Left: △E for 24 ordered orthorhombic crystal structure models with a single Si substituting P. The 6 crystallographic sites in the polyanionic chain are numbered in black. Type of anion site is labeled in color. Right: △E for 6 ordered orthorhombic crystal structures with 3 Si substituting P (12.5%).

skutterudite-type DOS has no band gap but a clear pseudogap in the vicinity of the Fermi level. In turn, the hypothetical orthorhombic polymorph's DOS clearly has a bandgap slightly above the Fermi level. One can assume that tuning the Si/P ratio in the latter structure may place the Fermi level at the top of valence band. The DOS for both Si-substituted structure types was calculated for the lowest energy ordered models from coloring studies and revealed that both phases have Fermi levels within the valence band, indicative of metallic behavior (Figure 6).

From the total energies of all four structures (Table S4), it was evident that the skutterudite-type structures (pristine and Si-substituted) were slightly lower in energy than the orthorhombic polymorphs with the same composition with ΔE of 21–29 meV/atom. Specifically, this supports the experimental observation that *c*-$RhSi_{0.3}P_{2.7}$ could be stabilized at higher temperatures by heating metastable *o*-$RhSi_{0.3}P_{2.7}$.

To summarize our experimental and computational findings: the chiral orthorhombic phase is a metastable compound, while the centrosymmetric cubic structure is a thermodynamically stable polymorph. The experimental unit cell volume of *o*-$RhSi_{0.3}P_{2.7}$ was 4% smaller than that for *c*-RhP_3 (489.60(3) $Å^3$ vs. 511.06 $Å^3$, respectively).[61] Computations corroborated this observation – for each polymorphic pair (*o*-RhP_3 and *c*-RhP_3, as well as *o*-$RhSi_xP_{3-x}$ and *c*-$RhSi_xP_{3-x}$), the relaxed unit cell volume of the orthorhombic phase was 5% smaller than the the one for cubic polymorph with the same composition (Table S4). This suggests that synthesis under applied pressure is a way to stabilize the orthorhombic polymorph. The total energy calculations reveal that the incorporation of Si did not provide additional energy stabilization for the metastable polymorph. From a chemical bonding point of view, an introduction of 10% of Si into the skutterudite structure should lead to random Si atomic placement in the P sublattice with the most probable new local fragments being $Rh(Si_1P_5)$ octahedra. In turn, the orthorhombic polymorph exhibited strong preference for specific Si placements in the P sublattice, thus introducing new *cis*-$Rh(Si_2P_4)$ and *fac*-$Rh(Si_3P_3)$ building blocks. Those local fragments are additionally stabilized due to the π-electron Rh→Si back donation (see above).

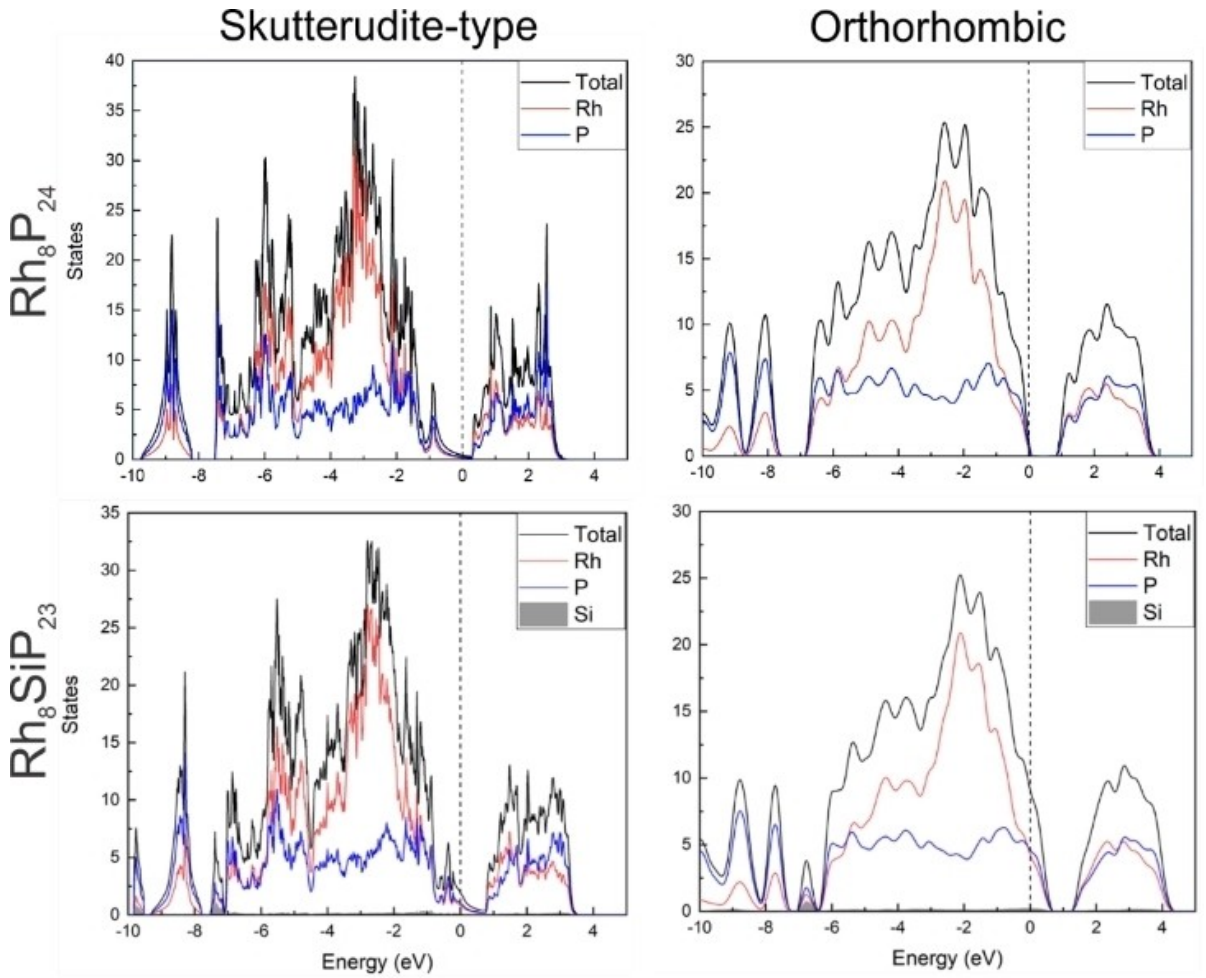

Figure 6. Density of states (DOS) for unsubstituted skutterudite-type and orthorhombic "Rh_8P_{24}" (*c*-RhP_3 and *o*-RhP_3) structures (top left, top right), as well as DOS for lowest energy structures of single Si-substituted skutterudite-type and orthorhombic "Rh_8SiP_{23}" (*c*-Rh_8SiP_{23} bottom left, *o*-Rh_8SiP_{23} bottom right). The Fermi level, indicated by the dashed line, is the reference energy.

Transport properties

Low temperatures (< 673 K) were required to sinter pellets of *o*-$RhSi_{0.3}P_{2.7}$ and avoid transformation of the metastable orthorhombic phase to the thermodynamically favored skutterudite phase. A low temperature and high pressure sintering profile resulted in pellets with a relative geometric density of ~56% for *o*-$RhSi_{0.3}P_{2.7}$ and ~92% for *c*-RhP_3. Thermal conductivity, Seebeck coefficient, and electrical resistivity were measured on these pellets (Figures S8 and 7). Thermal conductivity was much larger for RhP_3, reaching 8 W/m*K at room temperature, as compared to just above 2 W/m*K for *o*-$RhSi_{0.3}P_{2.7}$. High thermal conductivity is a common deterrent for using unfilled skutterudites as thermoelectrics because this results in a low figure-of-merit, zT.[62] The thermal conductivity of *o*-$RhSi_{0.3}P_{2.7}$ was lower, but it is unclear whether this is a result of different crystal structure, lower pellet density, or both. The Seebeck coefficients for both phases were positive, indicating holes as the main charge carriers (*p*-type), and increased linearly with temperature.

Lastly, a four-probe electrical resistivity measurement (Figure 7) shows *o*-$RhSi_{0.3}P_{2.7}$ to have temperature dependent semiconducting behavior. The bandgap was estimated to be ~0.05 eV using the high temperature region of the electrical resistivity and the relationship of $\ln(1/\rho) = (E_a/2k_BT)$, where E_a is the activation energy (bandgap) and k_B is the Boltzmann constant.[63] The change of structure from *o*-$RhSi_{0.3}P_{2.7}$ to *c*-$RhSi_{0.3}P_{2.7}$ resulted in a drastic change in properties. A sample of transformed *c*-$RhSi_{0.3}P_{2.7}$ showed nearly temperature-independent heavily doped semiconducting behavior. The resistivity further changed for the pristine *c*-RhP_3, which revealed metallic behavior based on electrical resistivity increasing linearly with temperature. Thus, a rearrangement of the crystal structure from a centrosymmetric skutterudite-type to chiral orthorhombic NCS structure lead to the opening of a bandgap and orders of magnitude changes in resistivity values. Our simple computational model predicted incomplete filling of the valence band for *o*-$RhSi_{0.3}P_{2.7}$ but DFT is known to underestimate localization effects for partially-disordered structures, as in the case of the high-temperature $LaSiP_3$ polymorph.[64]

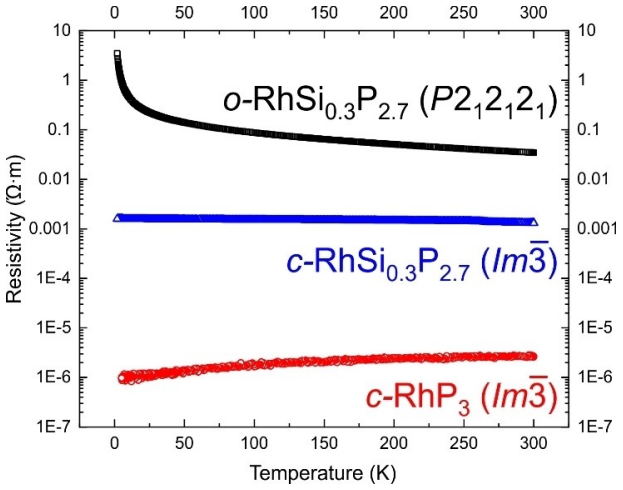

Figure 7. Temperature-dependent electrical resistivity measured from 2 to 280 K on sintered pellets of *o*-$RhSi_{0.3}P_{2.7}$ (black squares), *c*-$RhSi_{0.3}P_{2.7}$ (blue triangles), and *c*-RhP_3 (red circles).

Conclusion

Structural characterization of the novel compound, *o*-$RhSi_{0.3}P_{2.7}$ (space group $P2_12_12_1$) revealed the presence of unique polyanionic P/Si chains with nonsymmorphic and chiral symmetry, unlike 1D phosphorus chains observed in other metal phosphides. PXRD analysis (in situ and ex situ) revealed that *o*-$RhSi_{0.3}P_{2.7}$ irreversibly transformed into a silicon-containing skutterudite structure (space group $Im\bar{3}$) at 1273 K. Total energy calculations confirmed the metastable nature of *o*-$RhSi_{0.3}P_{2.7}$ as well as preference for Si at the highest coordinated sites in the polyanionic chains of the $P2_12_12_1$ structure. Electronic structure calculations predicted both the orthorhombic and cubic $RhSi_{0.3}P_{2.7}$ phases to be semimetals or metals, although transport measurements showed *o*-$RhSi_{0.3}P_{2.7}$ to be a narrow gap semiconductor in contrast to metallic RhP_3. A similar strategy used in this work may be applied to other centrosymmetric materials in the search for new nonsymmorphic and non-centrosymmetric materials with intriguing physical phenomena such as topological semimetals, superconductors, piezoelectric – just add a pinch of tetrel.

Acknowledgements

We would like to thank Professor Julia Zaikina (Iowa State University) for access to the SPS instrument and Professor Vitalij Pecharsky (US DOE Ames Laboratory) for the use of the arc-melting setup. This work was supported by the Ames Laboratory's Laboratory Directed Research and Development (LDRD) program (S. L., G. V., G. A., C. H., K. K.). G. A. is grateful to the Ames Laboratory Spedding Postdoctoral Fellowship for financial support. Solid-state NMR spectroscopy experiments (S. L. C. and A. J. R.) were supported by the U.S. Department of Energy (DOE), Office of Science, Basic Energy Sciences, Materials Science and Engineering Division. Ames Laboratory is operated for the U.S. DOE by Iowa State University under contract # DE-AC02-07CH11358. The authors would like to thank Dr. W. Xu and Dr. A. Yakovenko for help with conducting the in situ PXRD measurements at 17-BM (APS-ANL). This research used resources of the Advanced Photon Source, a U.S. Department of Energy (DOE) Office of Science User Facility operated for the DOE Office of Science by Argonne National Laboratory under Contract No. DE-AC02-06CH11357.

Conflict of Interest

The authors declare no conflict of interest.

Data Availability Statement

The data that support the findings of this study are available from the corresponding author upon reasonable request.

Keywords: chirality · crystal engineering · phase transitions · polymorphism · solid-phase synthesis

[1] D. Friedrich, H. R. Byun, S. Hao, S. Patel, C. Wolverton, J. I. Jang, M. G. Kanatzidis *J. Am. Chem. Soc.* **2020**, *142*, 17730–17742.
[2] L. Luo, D. Cheng, B. Song, L.-L. Wang, C. Vaswani, P. M. Lozano, G. Gu, C. Huang, R. H. J. Kim, Z. Liu, J.-M. Park, Y. Yao, K. Ho, I. E. Perakis, Q. Li, J. Wang, *Nat. Mater.* **2021**, *20*, 329–334.
[3] B. J. Wieder, B. Bradlyn, Z. Wang, J. Cano, Y. Kim, H.-S. D. Kim, A. M. Rappe, C. L. Kane, B. A. Bernevig, *Science* **2018**, *361*, 246–251.
[4] M. Kang, L. Ye, S. Fang, J.-S. You, A. Levitan, M. Han, J. I. Facio, C. Jozwiak, A. Bostwick, E. Rotenberg, M. K. Chan, R. D. McDonald, D. Graf, K. Kaznatcheev, E. Vescovo, D. C. Bell, E. Kaxiras, J. van den Brink, M. Richter, M. Prasad Ghimire, J. G. Checkelsky, R. Comin, *Nat. Mater.* **2020**, *19*, 163–169.
[5] Y. Wu, L.-L. Wang, E. Mun, D. D. Johnson, D. Mou, L. Huang, Y. Lee, S. L. Bud'ko, P. C. Canfield, A. Kaminski, *Nat. Phys.* **2016**, *12*, 667–671.
[6] J. Wang, K. Kovnir, *Nat. Photonics* **2018**, *12*, 382–383.
[7] Z. Ni, K. Wang, Y. Zhang, O. Pozo, B. Xu, X. Han, K. Manna, J. Paglione, C. Felser, A. G. Grushin, F. de Juan, E. J. Mele, L. Wu, *Nat. Commun.* **2021**, *12*, 154.
[8] R. A. Wiscons, Y. Cho, S. Y. Han, A. H. Dismukes, E. Meirzadeh, C. Nuckolls, T. C. Berkelbach, X. Roy, *J. Am. Chem. Soc.* **2021**, *143*, 109–113.
[9] C. Vaswani, J. H. Kang, M. Mootz, L. Luo, X. Yang, C. Sundahl, D. Cheng, C. Huang, R. H. J. Kim, Z. Liu, Y. G. Collantes, E. E. Hellstrom, I. E. Perakis, C. B. Eom, J. Wang, *Nat. Commun.* **2021**, *12*, 258.
[10] K. E. Woo, J. Wang, K. Wu, K. Lee, J.-A. Dolyniuk, S. Pan, K. Kovnir, *Adv. Funct. Mater.* **2018**, *28*, 1801589.
[11] J. Mark, J. Wang, K. Wu, J. G. Lo, S. Lee, K. Kovnir, *J. Am. Chem. Soc.* **2019**, *141*, 11976–11983.
[12] T. Yu, S. Wang, X. Zhang, C. Li, J. Qiao, N. Jia, B. Han, S.-Q. Xia, X. Tao, *Chem. Mater.* **2019**, *31*, 2010–2018.
[13] K. Zhong, C. Liu, M. Wang, J. Shi, B. Kang, Z. Yuan, J. Li, D. Xu, W. Shi, J. Yao, *Opt. Mater. Express* **2017**, *7*, 3571–3579.
[14] S. Lee, S. L. Carnahan, G. Akopov, P. Yox, L.-L. Wang, A. J. Rossini, K. Wu, K. Kovnir, *Adv. Funct. Mater.* **2021**, *31*, 2010293.
[15] H.-D. Yang, M.-Y. Ran, W.-B. Wei, X.-T. Wu, H. Lin, Q.-L. Zhu, *Chem. Asian J.* **2021**, *16 (21)*, 3299–3310.
[16] *Inorganic Crystal Structure Database, ICSD*, **2019**.
[17] S. J. Lee, J. Won, L.-L. Wang, D. Jing, C. P. Harmer, J. Mark, G. Akopov, K. Kovnir, *Chem. Eur. J.* **2021**, *27*, 7383–7390.
[18] M. Kirschen, H. Vincent, Ch. Perrier, P. Chaudouet, B. Chenevier, R. Madar, *Mater. Res. Bull.* **1995**, *30*, 507–513.
[19] P. Kaiser, W. Jeitschko, *Zeitschr. Naturforsch. B* **1997**, *52*, 462–468.
[20] Ch. Perrier, M. Kirschen, H. Vincent, U. Gottlieb, B. Chenevier, R. Madar, *J. Solid State Chem.* **1997**, *133*, 473–478.
[21] Ch. Perrier, H. Vincent, P. Chaudouët, B. Chenevier, R. Madar, *Mater. Res. Bull.* **1995**, *30*, 357–364.
[22] H. Vincent, J. Kreisel, Ch. Perrier, O. Chaix-Pluchery, P. Chaudouet, R. Madar, F. Genet, G. Lucazeau, *J. Solid State Chem.* **1996**, *124*, 366–373.
[23] J. Chen, C. Lin, G. Peng, F. Xu, M. Luo, S. Yang, S. Shi, Y. Sun, T. Yan, B. Li, N. Ye, *Chem. Mater.* **2019**, *31*, 10170–10177.
[24] J. Mark, K. Woo, W. Zhu, B. Ji, S. Lee, A. Adeyemi, S. Sen, K. Kovnir, *Chem. Mater.* **2021**, *33*, 4586–4595.
[25] W. M. Hurng, E. S. Peterson, J. D. Corbett, *Inorg. Chem.* **1989**, *28*, 4177–4180.
[26] J.-P. Fleurial, T. Caillat, A. Borshchevsky, in *AIP Conference Proceedings*, AIP, Kansas City, Missouri (USA), **1994**, pp. 40–44.
[27] M. Rull-Bravo, A. Moure, J. F. Fernández, M. Martín-González, *RSC Adv.* **2015**, *5*, 41653–41667.
[28] B. Chen, J.-H. Xu, C. Uher, D. T. Morelli, G. P. Meisner, J.-P. Fleurial, T. Caillat, A. Borshchevsky, *Phys. Rev. B* **1997**, *55*, 1476–1480.
[29] B. C. Sales, D. Mandrus, R. K. Williams, *Science* **1996**, *272*, 1325–1328.
[30] X. Shi, J. Yang, J. R. Salvador, M. Chi, J. Y. Cho, H. Wang, S. Bai, J. Yang, W. Zhang, L. Chen, *J. Am. Chem. Soc.* **2011**, *133*, 7837–7846.
[31] G. Xing, X. Fan, W. Zheng, Y. Ma, H. Shi, D. J. Singh, *Sci. Rep.* **2015**, *5*, 10782.
[32] G. A. Lamberton, R. H. Tedstrom, T. M. Tritt, G. S. Nolas, *J. Appl. Phys.* **2005**, *97*, 113715.
[33] G. S. Nolas, H. Takizawa, T. Endo, H. Sellinschegg, D. C. Johnson, *Appl. Phys. Lett.* **2000**, *77*, 52–54.
[34] >R. Gumeniuk, H. Borrmann, A. Ormeci, H. Rosner, W. Schnelle, M. Nicklas, Y. Grin, A. Leithe-Jasper, *Z. Kristallogr.* **2010**, *225*, 531–543.
[35] H. Fukuoka, *Crystals* **2017**, *7*, 381.
[36] R. Gumeniuk, W. Schnelle, H. Rosner, M. Nicklas, A. Leithe-Jasper, Y. Grin, *Phys. Rev. Lett.* **2008**, *100*, 017002.
[37] E. Bauer, A. Grytsiv, X.-Q. Chen, N. Melnychenko-Koblyuk, G. Hilscher, H. Kaldarar, H. Michor, E. Royanian, G. Giester, M. Rotter, R. Podloucky, P. Rogl, *Phys. Rev. Lett.* **2007**, *99*, 217001.
[38] P. Narang, C. A. C. Garcia, C. Felser, *Nat. Mater.* **2020**, *20*, 293—300 .
[39] S. Chadov, X. Qi, J. Kübler, G. H. Fecher, C. Felser, S. C. Zhang, *Nat. Mater.* **2010**, *9*, 541–545.
[40] H. Harima, K. Takegahara, *J. Phys. Condens. Matter* **2003**, *15*, S2081–S2086.
[41] H. Luo, J. W. Krizan, L. Muechler, N. Haldolaarachchige, T. Klimczuk, W. Xie, M. K. Fuccillo, C. Felser, R. J. Cava, *Nat. Commun.* **2015**, *6*, 6489.
[42] B. Khan, H. A. R. Aliabad, Saifullah, S. Jalali-Asadabadi, I. Khan, I. Ahmad, *J. Alloys Compd.* **2015**, *647*, 364–369.
[43] K. Takegahara, H. Harima, *Physica B+C* **2003**, *328*, 74–76.
[44] M. P. Hanrahan, A. Venkatesh, S. L. Carnahan, J. L. Calahan, J. W. Lubach, E. J. Munson, A. J. Rossini, *Phys. Chem. Chem. Phys.* **2017**, *19*, 28153–28162.
[45] N. M. Szeverenyi, M. J. Sullivan, G. E. Maciel, *J. Magn. Reson.* **1982**, *47*, 462–475.
[46] D. Sakellariou, S. P. Brown, A. Lesage, S. Hediger, M. Bardet, C. A. Meriles, A. Pines, L. Emsley, *J. Am. Chem. Soc.* **2003**, *125*, 4376–4380.
[47] E. Bekaert, J. Bernardi, S. Boyanov, L. Monconduit, M.-L. Doublet, M. Ménétrier, *J. Phys. Chem. C* **2008**, *112*, 20481–20490.
[48] I. Furo, I. Bakonyi, K. Tompa, E. Zsoldos, I. Heinmaa, M. Alla, E. Lippmaa, *J. Phys. Condens. Matter* **1990**, *2*, 4217.
[49] C. Stinner, Z. Tang, M. Haouas, T. Weber, R. Prins, *J. Catal.* **2002**, *208*, 456–466.
[50] J. Fulmer, O. I. Lebedev, V. V. Roddatis, D. C. Kaseman, S. Sen, J.-A. Dolyniuk, K. Lee, A. V. Olenev, K. Kovnir, *J. Am. Chem. Soc.* **2013**, *135*, 12313–12323.
[51] H. G. von Schnering, W. Hoenle, *Chem. Rev.* **1988**, *88*, 243–273.
[52] R. Pöttgen, W. Hönle, H. G. von Schnering, in *Encyclopedia of Inorganic and Bioinorganic Chemistry* (Ed.: R. A. Scott), John Wiley & Sons, Ltd, Chichester, UK, **2011**, pp. 4255–4307.
[53] M. Bawohl, T. Nilges, *Z. Anorg. Allg. Chem.* **2015**, *641*, 304–310.
[54] H.-G. von Schnering, D. Vu, *J. Less-Common Met.* **1986**, *116*, 259–270.
[55] W. Hönle, R. Kremer, H. G. von Schnering, *Z. Krist. – Cryst. Mater.* **1987**, *179*, 443–454.
[56] R. Rühl, W. Jeitschko, *Acta Crystallogr. Sect. B* **1982**, *38*, 2784–2788.
[57] J. Dolyniuk, P. S. Whitfield, K. Lee, O. I. Lebedev, K. Kovnir, *Chem. Sci.* **2017**, *8*, 3650–3659.
[58] J. Wang, O. I. Lebedev, K. Lee, J.-A. Dolyniuk, P. Klavins, S. Bux, K. Kovnir, *Chem. Sci.* **2017**, *8*, 8030–8038.
[59] J. Wang, Y. He, N. E. Mordvinova, O. I. Lebedev, K. Kovnir, *Chem* **2018**, *4*, 1465–1475.
[60] G. J. Miller, *Eur. J. Inorg. Chem.* **1998**, *1998*, 523–536.
[61] S. Rundqvist, *Nature* **1960**, *185*, 31–32.
[62] Z.-Y. Liu, J.-L. Zhu, X. Tong, S. Niu, W.-Y. Zhao, *J. Adv. Ceram.* **2020**, *9*, 647–673.
[63] C. Kittel, *Introduction to Solid State Physics*, Wiley, Hoboken, N. J., **1996**.
[64] G. Akopov, J. Mark, G. Viswanathan, S. J. Lee, B. C. McBride, J. Won, F. A. Perras, A. L. Paterson, B. Yuan, S. Sen, A. N. Adeyemi, F. Zhang, C.-Z. Wang, K.-M. Ho, G. J. Miller, K. Kovnir, *Dalton Trans.* **2021**, *50*, 6463–6476.

Manuscript received: December 3, 2021
Accepted manuscript online: December 9, 2021
Version of record online: January 12, 2022